Journal of *Marine Science and Engineering*

MDPI

Article

Numerical Investigation on Aerodynamic Characteristics of Dual-Rotor Wind Turbines

Kai Wang [1,2,*], Tianhui Liu [1], Yuanchen Wan [1], Muk Chen Ong [3] and Tiecheng Wu [1,2]

[1] School of Ocean Engineering and Technology, Sun Yat-sen University, Zhuhai 519000, China
[2] Southern Marine Science and Engineering Guangdong Laboratory (Zhuhai), Zhuhai 519000, China
[3] Department of Mechanical and Structural Engineering and Materials Science, University of Stavanger, 4036 Stavanger, Norway
* Correspondence: wangkai25@mail.sysu.edu.cn

Abstract: Improving power output and reducing costs are crucial to the sustainable development of offshore wind power. In the present study, a dual-rotor wind turbine (DRWT) is proposed to improve wind energy capture efficiency by adding an auxiliary rotor behind the main rotor. The two rotors can be the same size or different sizes. This will result in different aerodynamic characteristics for DRWTs. In this paper, the NREL Offshore Baseline-5 MW and the NREL 750 kW single-rotor wind turbines (SRWTs) are used to configure three different types of DRWTs. The power output and wake characteristics of three different DRWTs with co-rotating (CO-DRWT) and counter-rotating (CR-DRWT) configurations on an actual scale are compared. The Reynolds-averaged Navier–Stokes (RANS) model with k-ω SST (shear stress transport model) is used to simulate the unsteady flow generated by the DRWT's rotation. The present numerical results show that the power coefficient of the 5 MW-5 MW CO-DRWT can reach 1.22 times that of the 5 MW SRWT. Moreover, a faster wake velocity deficit recovery is found in the 5 MW-5 MW DRWTs because the high-velocity flow caused by the merging and mixing of the trailing vortices of the 5 MW-5 MW DRWTs brings an energy supplement to the wake velocity deficit.

Keywords: horizontal-axis wind turbine (HAWT); dual-rotor wind turbine; computational fluid dynamics (CFD); aerodynamics characteristics; wake flow characteristics

check for updates

Citation: Wang, K.; Liu, T.; Wan, Y.; Ong, M.C.; Wu, T. Numerical Investigation on Aerodynamic Characteristics of Dual-Rotor Wind Turbines. *J. Mar. Sci. Eng.* **2022**, *10*, 1887. https://doi.org/10.3390/jmse10121887

Academic Editor: Unai Fernandez-Gamiz

Received: 31 October 2022
Accepted: 28 November 2022
Published: 4 December 2022

Publisher's Note: MDPI stays neutral with regard to jurisdictional claims in published maps and institutional affiliations.

Copyright: © 2022 by the authors. Licensee MDPI, Basel, Switzerland. This article is an open access article distributed under the terms and conditions of the Creative Commons Attribution (CC BY) license (https://creativecommons.org/licenses/by/4.0/).

1. Introduction

Wind energy is a kind of renewable energy with promising prospects [1,2]. The utilization of wind energy can solve the problem of energy shortages, reduce the dependence on fossil energy and optimize the energy structure [3]. The wind power industry is growing rapidly worldwide; the global cumulative wind power capacity now reaches 743 GW [4]. Researchers have carried out experimental and numerical studies on different concepts of wind energy conversion devices, including various horizontal-axis wind turbines and vertical-axis wind turbines [5–7]. Considering the high cost of wind power conversion devices, especially floating wind turbines, increasing power output and reducing the costs are the keys to promoting the use of wind turbines.

The horizontal-axis single-rotor wind turbine is the most widely used wind energy conversion device for utilizing wind energy. According to the Betz theory, the limit of the power coefficient of a single-rotor wind turbine (SRWT) is 0.593 in an ideal situation [8]. However, the design of the blades should also be given priority to bear the bending moment and torque caused by the wind load and the weight of the blades, so parts of the blades ranging from the hub to the blade tip within the distance of 0 R to 0.25 R (R represents the radius of the blade) are ineffective in capturing the wind energy. Taking a 5 MW wind turbine as an example, the airfoil section from the hub to the blade tip within 0–8 m is circular, so does not have any ability to capture wind energy. In fact, the wind energy power coefficient of the horizontal-axis SRWT is limited to a range of only 40% to 50%

according to Tony et al. [9]. Hence, improving the capture efficiency of wind energy is highly attractive for reducing the cost of offshore wind farms.

Considering the power efficiency limit of the SRWT, the DRWT is proposed to improve wind energy capture efficiency. The concept of dual-rotor turbines was initially applied to the propellers of ships and the wings of helicopters and was applied later to wind turbines. The main feature of the DRWT is the addition of an auxiliary rotor to the original SRWT, as shown in Figure 1. The auxiliary rotor increases the power output by capturing the energy in the wake of the front rotor. The DRWT can effectively improve the utilization efficiency of wind energy. Newman et al. [10] showed that the ideal maximum power coefficient of a wind turbine having two rotors can reach 64% based on an analysis with a uniform inflow factor through tandem actuator discs. The main rotor and the auxiliary rotor of the DRWT can be composed of two rotors of the same size or different sizes. The main rotor and the auxiliary rotor of the DRWT can be mounted on the same side of the nacelle or on two sides of the nacelle separately. Meanwhile, DRWTs can be divided into having either a co-rotating (CO-DRWT) or counter-rotating configuration (CR-DRWT). Therefore, DRWTs have had various configurations.

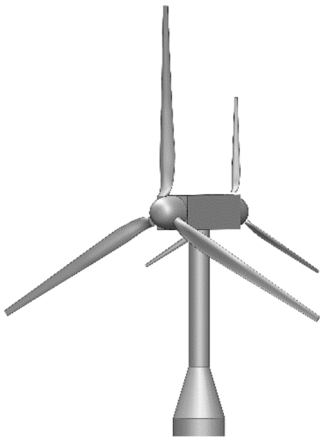

Figure 1. Illustration of a dual-rotor wind turbine.

Current state-of-art studies on the DRWT focus on comparing the increase in the power coefficient and the wake characteristics with those of the SRWT. Ahmet et al. [11] studied a DRWT using a wind tunnel test combined with particle image velocimetry (PIV) measurements. The power output and wake characteristics of the DRWT were quantified and compared with those of the SRWT. The DRWT, composed of the same type of rotors, can provide 60% more power. Wang et al. [12] studied a DRWT composed of two rotors with different diameters based on PIV measurements. The aerodynamic force and power output of the two rotors were compared. It was found that the aerodynamic force and power coefficient of CR-DRWTs were increased by 13.3% and 7.2%, respectively. Rosenberg et al. [13] designed a DRWT that consisted of two different types of rotors on the same side of the nacelle and used the RANS model to optimize the design of the DRWT. Lee et al. [14] used the vortex lattice method to compare the aerodynamic characteristics of the NREL phase-VI SRWT and a CR-DRWT mounted by two NREL phase-VI rotors.

Experiments and simulations of DRWTs show that the main advantage of the DRWT is the improvement of the power coefficient. Another advantage of DRWTs is that the range of cut-in and cut-out wind speeds can be widened. This means a better capture of low-quality wind power [15,16].

A DRWT generally has a higher power coefficient than that of an SRWT. Power output and aerodynamic performance of DRWTs in wind farms are also the focus of current research studies. Ahmadreza et al. [17] investigated the power output of a wind farm with 48 large wind turbines, similar to the one in Lillgrund, Sweden, using large eddy simulations in combination with an actuator line model. It was found that the wind farm composed of DRWTs generated 22.6% more power than the wind farm composed of SRWTs.

Apart from a higher power efficiency, it was found that the negative effect of the front wind turbine on the rear wind turbine in a farm composed of DRWTs was less than that in a wind farm composed of SRWTs.

When studying the aerodynamic performance of a DRWT through wind tunnel experiments, the DRWT geometric model needs to be scaled down. However, the geometric similarity and motion similarity cannot be satisfied at the same time when the model is scaled down. It cannot fully represent the flow characteristics of the actual-scale DRWTs. Therefore, it is necessary to study an actual scale DRWT to get the flow characteristics and explain the DRWT's advantages in wind farms. Hence, the computational fluid dynamics (CFD) method can be a suitable method to study actual-scale DRWTs considering the huge dimension and the complex flow characteristics [18,19]. In addition, DRWTs have been studied in comparison with SRWTs. However, to the authors' knowledge, there is a lack of comparative studies between different DRWTs with different configurations.

In this paper, NREL Offshore Baseline-5 MW and NREL 750 kW wind turbines are used to compose three different DRWTs (5 MW-5 MW, 5 MW-750 kW and 750 kW-5 MW), and the three DRWTs at rated working conditions with both co-rotating and counter-rotating configurations are simulated in an actual-scale model using the CFD method. This study aimed to focus on the comparative study of power coefficients and wake characteristics of different DRWTs on an actual scale. The actual-scale DRWTs are used to avoid any scaling effect on the power and wake characteristics, which may exist in previous studies for scaled-down rotors.

This paper is organized as follows: Section 1 introduces the advantages of and current research on DRWTs. Section 2 describes the DRWTs' geometry model used in this study. Section 3 presents the theory of the numerical model, the boundary settings and the grid settings for the numerical solution. In Section 4, the power coefficient and thrust coefficient of DRWTs and the wake characteristics are studied in detail. Section 5 provides a summary of this study.

2. Wind Turbine Geometry

The NREL Offshore Baseline-5 MW wind turbine and the NREL 750 kW Wind PACT baseline wind turbine were selected as the main rotor and the auxiliary rotor for DRWTs. The main information on these two wind turbines is open access and has been used in research on wind turbine dynamics [20,21]. The blade cross-sections of the 5 MW turbine adopted the DU and NACA airfoils, and the blade cross-sections of the 750 kW turbine adopted the S airfoil. The detailed parameters of the 5 MW and 750 kW turbines are given in Table 1.

Table 1. Single-rotor turbine wind parameters.

Items	5 MW Wind Turbine	750 kW Wind Turbine
Blade quantity	3	3
Diameter	126 m	50 m
Rated rotational speed	12.1 rpm	28.648 rpm
Rated wind speed	11.4 m/s	11 m/s

Three types of DRWTs were mounted on 5 MW and 750 kW wind turbines, i.e., 5 MW-5 MW, 5 MW-750 kW and 750 kW-5 MW DRWTs, as shown in Figure 2. Each DRWT adopted co-rotating and counter-rotating configurations. Figure 2a shows 5 MW-5 MW DRWT, Figure 2b shows 5 MW-750 kW DRWT and Figure 2c shows 750 kW-5 MW DRWT. Figure 3 shows the blade details for co-rotating and counter-rotating configurations.

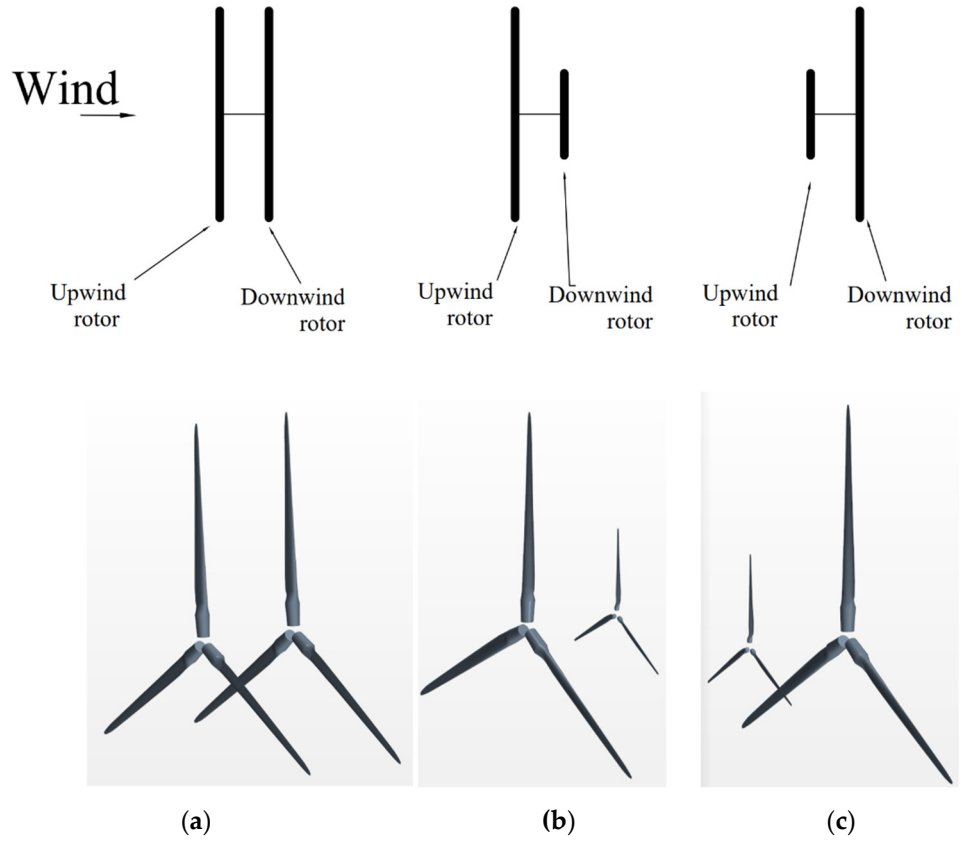

Figure 2. DRWTs: (**a**) 5 MW-5 MW DRWT; (**b**) 5 MW-750 kW DRWT; (**c**) 750 kW-5 MW DRWT.

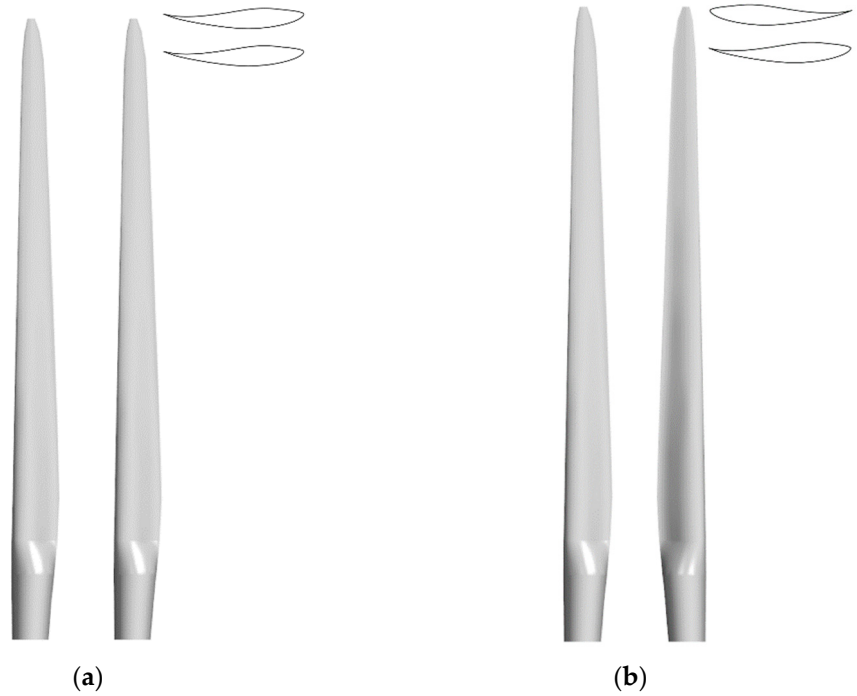

Figure 3. (**a**) Blade details of co-rotating configurations; (**b**) blade details of counter-rotating configurations.

3. Numerical Model

3.1. Numerical Method and Basic Formula

Many numerical methods can be applied to study the aerodynamic performance of wind turbines, including the blade element theory, vortex lattice method and CFD

method [22–24]. The finite volume-based CFD software STAR-CCM+ was used in this study. The k-ω SST RANS model has good applicability to simulate complex flow phenomena (separated flow, rotation) as well as fully developed turbulent flows around airfoils and rotating blades [25–28]. Hence, the k-ω SST RANS model was used to simulate the flow characteristics of the presented dual-rotor wind turbine. The SIMPLE (Semi-Implicit Method for Pressure-Linked Equations) algorithm and the first-order spatial and temporal schemes were used in this study.

The rotor was given a certain rotating speed. Incompressible fluid was applied in the present simulations since the Mach number of the flow in the present study was less than 0.3. The governing equations are shown as follows [29]:

$$\nabla \cdot \mathbf{u} = 0, \tag{1}$$

$$\rho\left(\frac{\partial \mathbf{u}}{\partial t} + \nabla \cdot (\mathbf{u}\mathbf{u})\right) = -\nabla p + \nabla \cdot \mu\left(\nabla \mathbf{u} + \nabla \mathbf{u}^T\right) + \rho \mathbf{g}, \tag{2}$$

where ρ is the density, $\mathbf{u}$ is the velocity, $\mathbf{g}$ is the acceleration due to gravity and μ is the dynamic viscosity.

In the process of analysis, the power coefficient, thrust coefficient and power density ratio are defined as follows.

Thrust coefficient:

$$C_T = \frac{2T}{\rho A {U_\infty}^2}, \tag{3}$$

where T is the rotor thrust, ρ is the density (for a wind turbine this is 1.29 kg/m^3), A is the area of the disk formed by the rotor rotation and U_∞ is the incoming flow velocity.

Power coefficient:

$$C_P = \frac{2P}{\rho A {U_\infty}^3}, \tag{4}$$

where P is the rotor power, and A is the area of the disk formed by the rotor rotation.

For DRWT systems:

$$C_{Tdual} = \frac{2(T_1 + T_2)}{\rho A {U_\infty}^2}, \tag{5}$$

where T_1 is the thrust of the upwind rotor of the DRWT, and T_2 is the thrust of the downwind rotor of the DRWT.

$$C_{Pdual} = \frac{2(P_1 + P_2)}{\rho A {U_\infty}^3}, \tag{6}$$

where P_1 is the power output of the upwind rotor of the DRWT, and P_2 is the power output of the downwind rotor of the DRWT.

In order to compare the power coefficient of the DRWT fairly, especially when the main rotor and the auxiliary rotor are composed of 5 MW and 750 kW which have different diameters, in this study, the power density ratio is used as:

$$C_{PS} = \frac{P}{S}, \tag{7}$$

where P is the power output, and S is the sum of the projected areas of blades.

3.2. Boundary Conditions and Grid Settings

The computational settings, including boundary conditions and grid resolutions, are shown in Figures 4 and 5. The computational domain consisted of a rectangular background region and wind turbine rotation regions. The height and width of the background region were 3D, the inlet was located in 3D on the rotor, and the outlet was located in 6 D downstream of the center of the upwind rotor. The inlet was set to a constant wind speed of 11.4 m/s as the rated working wind speed [20,21], and the outlet was set as a pressure outlet.

The computational domain was discretized by structured trimmer grids, and, in order to capture the flow around the blade and trailing vortices accurately, it was necessary to refine the grids around the rotor and the grids at the back of the rotor blade tips. Boundary layer grids were created in the peripheral area of the blade. The total length of the boundary layer grid was 0.02 m, which was divided into 9 grids, and the ratio between two neighboring cells was 1.5. The Y plus value of blades was less than 4. According to the technical literature, the rotor speed was set to 12.1 rpm for 5 MW and 28.648 rpm for 750 kW [20,21] as rated working conditions, and the rotor speed was not adjusted for the DRWTs.

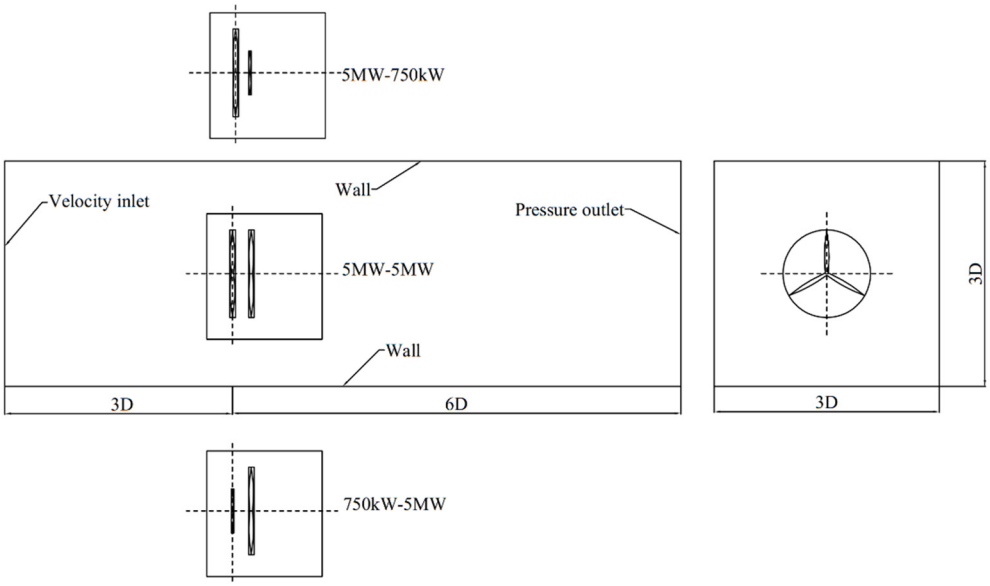

Figure 4. Sketch of the computational domain.

3.3. Mesh Convergence

Figure 6 presents the grid convergence based on the thrust force values of 5 MW SRWT and 750 kW SRWT versus the number of grids. Three different sizes of grids were used to test the grid convergence. There were no noticeable differences between the thrust force values of the two turbines with different grid settings. The stable numerical results of thrust prove that the grid setting was reasonable. The number of grids for a DRWT is the sum of the corresponding single wind turbines. In the following simulation, the number of 5 MW turbine grids is 7.12 million, the number of 750 kW turbine grids is 7.56 million, the number of 5 MW-5 MW DRWT grids is 14.02 million, and the number of DRWT grids composed of 5 MW and 750 kW SRWT is 10.88 million grids.

The results of 5 MW and 750 kW SRWTs were compared with the rated power output given by NREL to verify the reliability and accuracy of the simulation method, as given in Table 2. An error value of 10% was considered an acceptable range. There is no available published prototype of the DRWT with detailed hub and nacelle information. Therefore, the modeling of the DRWTs in this study does not include the hub and nacelle effects. Lee, Son and Lee [30] studied DRWTs composed of a 2-blade rotor using the free wake vortex lattice method without the hub and nacelle parts.

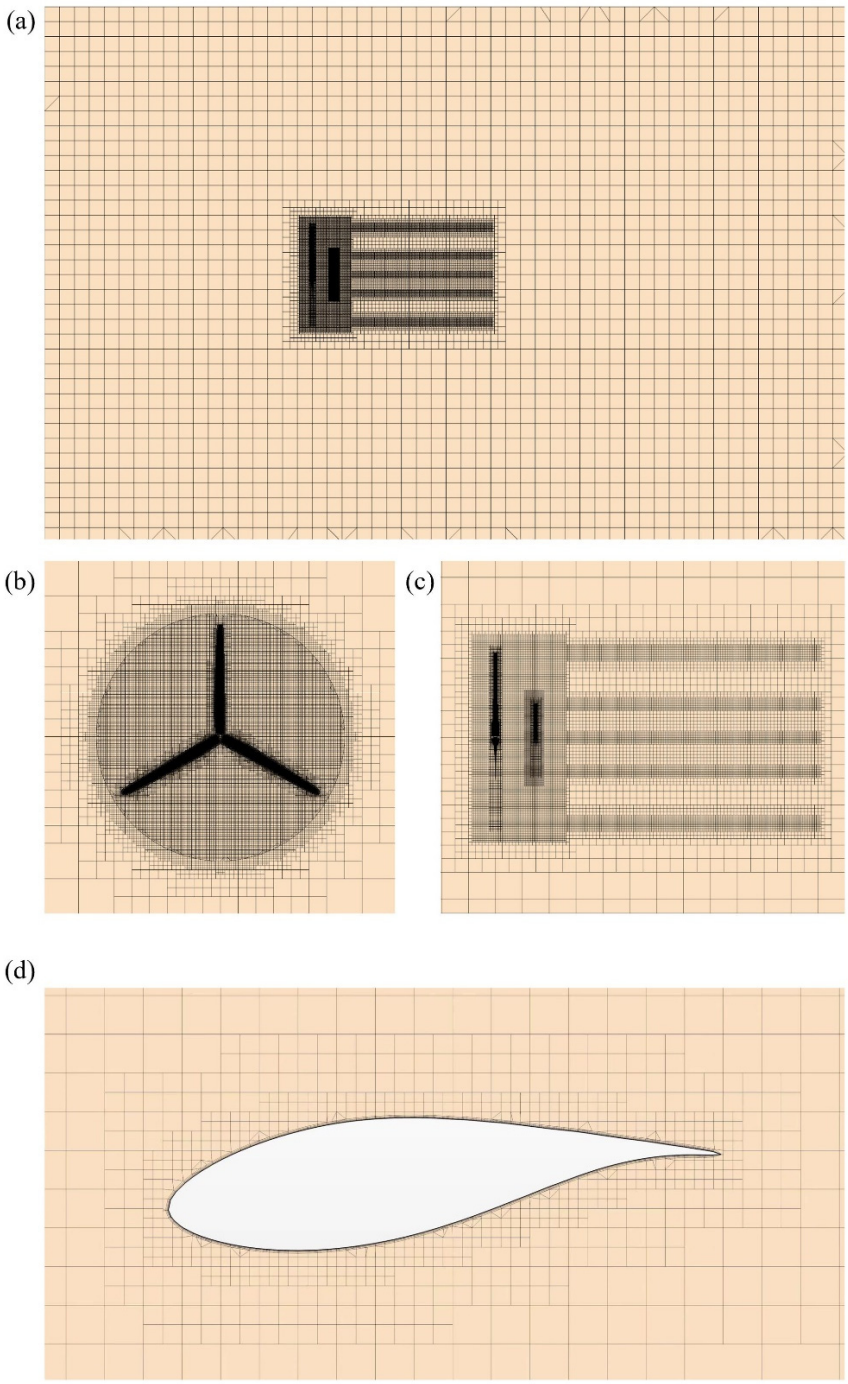

Figure 5. (**a**) Side view of the mesh in the entire computation domain; (**b**) front view of the mesh around the rotor; (**c**) side view of the mesh around the rotor; (**d**) boundary layer mesh positioned on a blade.

Table 2. Power calculation of 5 MW wind turbine and 750 kW wind turbine.

Items	5 MW Wind Turbine	750 kW Wind Turbine
Calculated Power	4,898,581.587 W	690,457.7664 W
Rated power	5 MW	750 kW
Error value	2.0%	7.9%

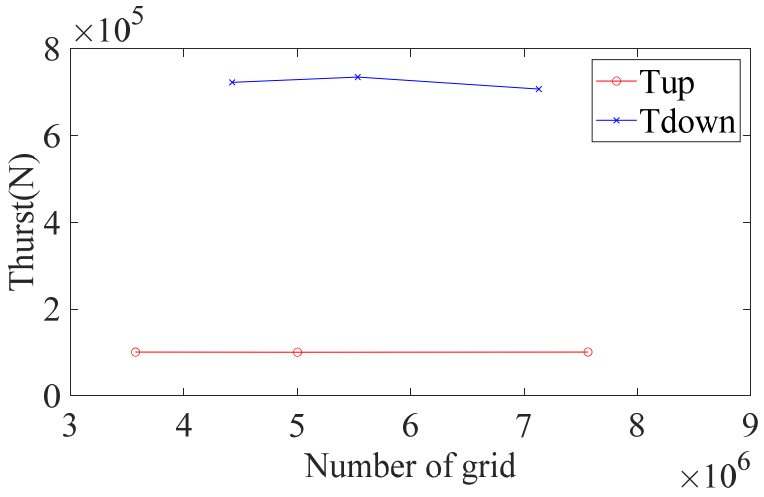

Figure 6. Grid convergence.

4. Results and Discussion

4.1. Power Coefficient and Thrust Coefficient

Previous studies [11,12] have shown that auxiliary rotors in DRWTs can improve the power coefficient by utilizing the wind energy in the wake at the root of the main rotor. Therefore, 5 MW-5 MW, 5 MW-750 kW and 750 kW-5 MW CO-DRWT and CR-DRWT were modeled in the present study. The power coefficients of each DRWT were extracted and compared. The result of the power coefficient of 5 MW SRWT was 0.411. This result was used to normalize the power coefficient of DRWTs and the power coefficients of the upwind rotors and downwind rotors. Figure 7 presents the normalized power coefficients of 5 MW-5 MW, 5 MW-750 kW and 750 kW-5 MW CO-DRWT and CR-DRWT. The power coefficient result of the 750 kW SRWTs was also used to normalize the power coefficient of the 750 kW auxiliary rotor in each DRWT, and the normalized results of the 750 kW auxiliary rotor are shown in Figure 8.

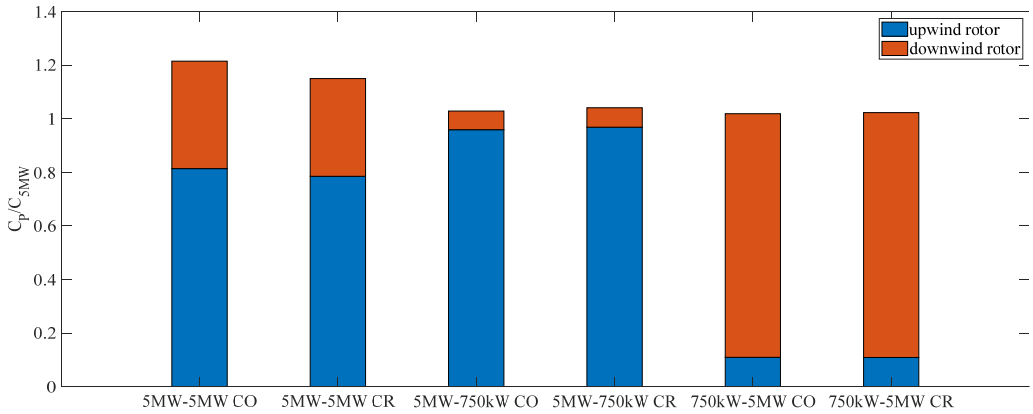

Figure 7. Normalized power coefficient of DRWTs.

The power coefficients of all DRWTs had different increases compared with the power coefficient of the 5 MW SRWT. The power coefficient of 5 MW-5 MW DRWTs was much higher than that of the DRWTs composed of 750 kW and 5 MW wind turbines. The power coefficient of the 5 MW-5 MW CO-DRWT is 1.22 times that of the 5 MW SRWT. The power coefficient of DRWTs composed of 750 kW and 5 MW did not increase as obviously as that of DRWTs composed of 5 MW and 5 MW. The power coefficients of 5 MW-750 kW and 750 kW-5 MW CO-DRWT or CR-DRWT increased about 1–3% compared with that of the 5 MW SRWT. This is consistent with Wang's [12] wind tunnel experimental results. There was a slight difference in the normalized power coefficient between 5 MW-750 kW DRWTs

and 750 kW-5 MW DRWTs; the power output performance of the DRWTs using a 5 MW rotor as the upwind rotor is better than that of the DRWTs using a 750 kW rotor as the upwind rotor, whether in a co-rotation or counter-rotation configuration.

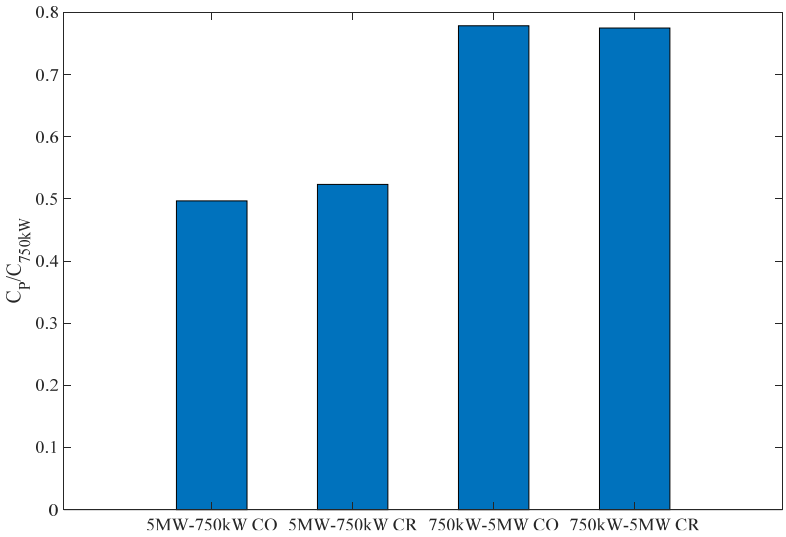

Figure 8. Normalized power coefficient of 750 kW rotor of DRWTs.

Individual power coefficients of the main rotor and the auxiliary rotor of the DRWTs are also given in Figure 7. The power output of the main rotor and the auxiliary rotor of a DRWT decreased compared with that of the corresponding SRWTs. The power output reduction of the downwind rotor was more severe than that of the upwind rotor. The power output of the downwind rotor of the 5 MW-5 MW CR-DRWT decreased most seriously: reduced to 36% of the power output of the 5 MW SRWT. This is mainly due to the attenuation of wind speeds when the upwind rotor captures wind energy.

Meanwhile, the power coefficients of the upwind rotors also had a slight decrease compared with those of the corresponding SRWTs. The power coefficients of the upwind rotors of the 5 MW-5 MW CO-DRWT, 5 MW-5 MW CR-DRWT, 750 kW-5 MW CO-DRWT and 750 kW-5 MW CR-DRWT were reduced to about 80% of the corresponding SRWT, while the upwind rotors' power coefficients of the 5 MW-750 kW CO-DRWT and CR-DRWT were reduced to about 96% of the corresponding SRWT. The power output decrease of the upwind rotor was caused by the negative influence of the downwind rotor when the upwind rotor and the downwind rotor rotated together. The shadow formed by the rotation of the downwind rotor blocks the wake flow of the upwind rotor, and this causes a power coefficient decrease in the upwind rotor. The negative influence is related to the rotating disk area formed by the downwind rotor. The 5 MW rotor was used in both the 5 MW-5 MW CO-DRWT and 5 MW-750 kW CO-DRWT; the individual upwind 5 MW rotors' power coefficient was reduced to 81% and 96% of that of the 5 MW SRWT, and the 5 MW-5 MW CR-DRWT and 5 MW-750 kW CR-DRWT have a similar tendency. This is because the 5 MW-750 kW CO-DRWT and CR-DRWT use a 750 kW rotor, which has a smaller rotating disk area than the downwind rotor.

In the following section, to further explain how to evaluate the negative effects between the downwind rotor and the upwind rotor, this study adopted the power solidity ratio to compare the performance of different DRWTs. The power solidity ratio is defined as the power coefficient divided by the projected area of the total blade sum of the upwind rotor and the downwind rotor. The power solidity ratio of the 5 WM SRWT was used to normalize the power coefficient of DRWTs. There was a large gap between the power output of 5 MW and 750 kW single-rotor wind turbines. Only comparing the power coefficient of DRWTs cannot show which DRWT has better performance. Lee et al. [14] used solidity (the ratio of total blade area to rotor disk area) as an evaluation index to compare the power performance of DRWTs. This study proposed a comparison of the

power performance of 5 MW-5 MW, 5 MW-750 kW, and 750 kW-5 MW CO-DRWTs and CR-DRWTs with the CPS of DRWTs. The CPS of the 5 MW SRWT was used to normalize the CPS of DRWTs. Figure 9 gives the result of the normalized CPS of CO-DRWTs and CR-DRWTs.

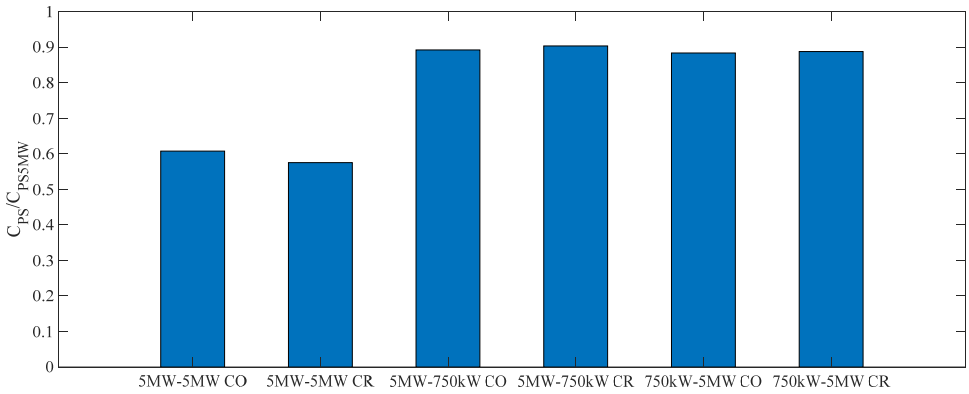

Figure 9. Normalized CPS of DRWTs.

As previously mentioned, the 5 MW-5 MW DRWT had the highest power coefficient among all DRWTs, but that does not mean it had the best performance. The 5 MW wind turbine had a blade radius of 63 m, which means a larger rotating disk area and larger wind capture area than the 750 kW SRWT. It can be seen from Figure 9 that the energy capture rate per unit area of DRWTs with the 750 kW auxiliary rotor is much higher than that of DRWTs with the 5 MW auxiliary rotor. As explained above, the negative influence caused by the interference between the upwind rotor and the downwind rotor is correlated with the rotating disk area formed by the downwind rotor. The 5 MW-750 kW DRWTs had the best energy capture rate per unit area among these six configurations. This is due to the 750 kW rotor being arranged as the downwind rotor, which had a less negative impact on the 5 MW upwind rotor.

Table 3 shows the thrust coefficients of the 5 MW single-rotor wind turbine and three types of DRWTs in co-rotation and counter-rotation. The auxiliary rotor of the DRWTs increased the power output and brought additional aerodynamic thrust, which requires a stronger supporting structure. The increase in thrust of DRWTs is consistent with the increase in the power coefficient of the DRWT. The thrust coefficients of the 5 MW-5 MW CO-DRWT were 59.8% higher than those of the 5 MW SRWT. The huge increase in the aerodynamic load will undoubtedly incur a higher cost for the structure. By looking at the comparison shown in Table 3, the 750 kW-5 MW CR-DRWT seems to be a more reasonable choice. The thrust coefficients of the 5 MW-750 kW and 750 kW-5 MW DRWTs increased by about 5–8%. The auxiliary 750 kW rotor of the DRWT enhanced the power output with a small increase in the average wind load. It is of great interest to mention the cost increase due to the added rotor of DRWTs. Moreover, the increase in the aerodynamic thrust of a DRWT requires a more robust supporting structure, which also leads to a cost increase. In the presented study, the power density ratio was used to evaluate the economy by summing up the rotating disk area, which can reflect the benefits of six different DRWTs. However, the rotating disk area is more related to the blade, which can only represent the cost of the blades of the DRWTs. The overall manufacturing cost of the DRWTs is difficult to evaluate through a single index due to the design of multiple components such as the blade, hub and tower.

From the point of view of generated power in a wind farm, based on Ahmadreza's study, a wind farm with 48 wind turbines composed of DRWTs was found to produce 22.6% more power than a wind farm composed of 48 SRWTs. The balance between the increase in cost and the increase in power output needs to be evaluated economically.

Table 3. Thrust coefficients of DRWTs.

System	C_T
5 MW	0.677
5 MW-5 MW CO	1.082
5 MW-5 MW CR	1.039
5 MW-750 kW CO	0.727
5 MW-750 kW CR	0.726
750 kW-5 MW CO	0.706
750 kW-5 MW CR	0.706

4.2. Velocity Distribution in Wake Flow

Figure 10 shows the longitudinal velocity distribution profile in the wake flow of DRWTs, and Figure 11 shows the vertical distribution of the wake velocity in 1 D distance, 2 D distance and 3 D distance (D is the rotor diameter of a 5 MW wind turbine) from the upwind rotor. It can be seen from Figure 10 that there is a velocity deficit region in the wake of DRWTs for all cases. It can be observed in Figure 11 that the velocity deficit region is mainly distributed in the wake area where the upwind rotor and the downwind rotor overlap. The velocity deficit in the wake region is due to the energy captured by the rotors. The downwind rotor captures the residual wind energy in the upwind rotor's wake so as to cause an obvious velocity deficit in the wake region. Hence, the high efficiency of wind energy capture by DRWT is observed.

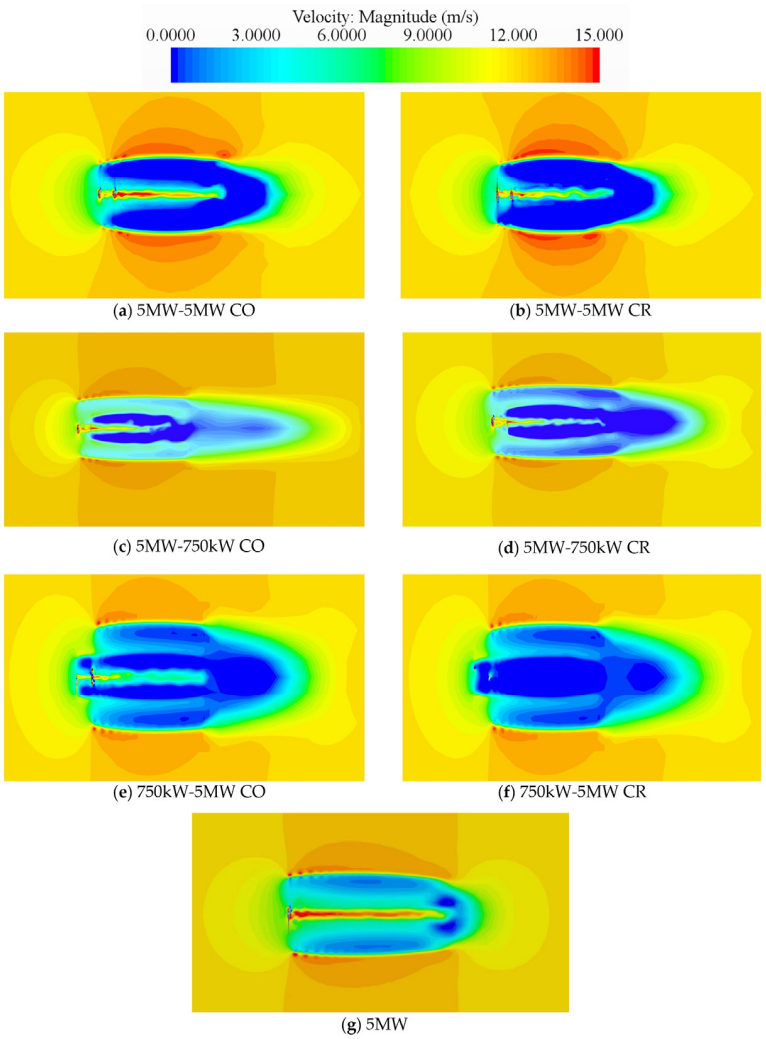

Figure 10. Velocity distributions in the wake flow.

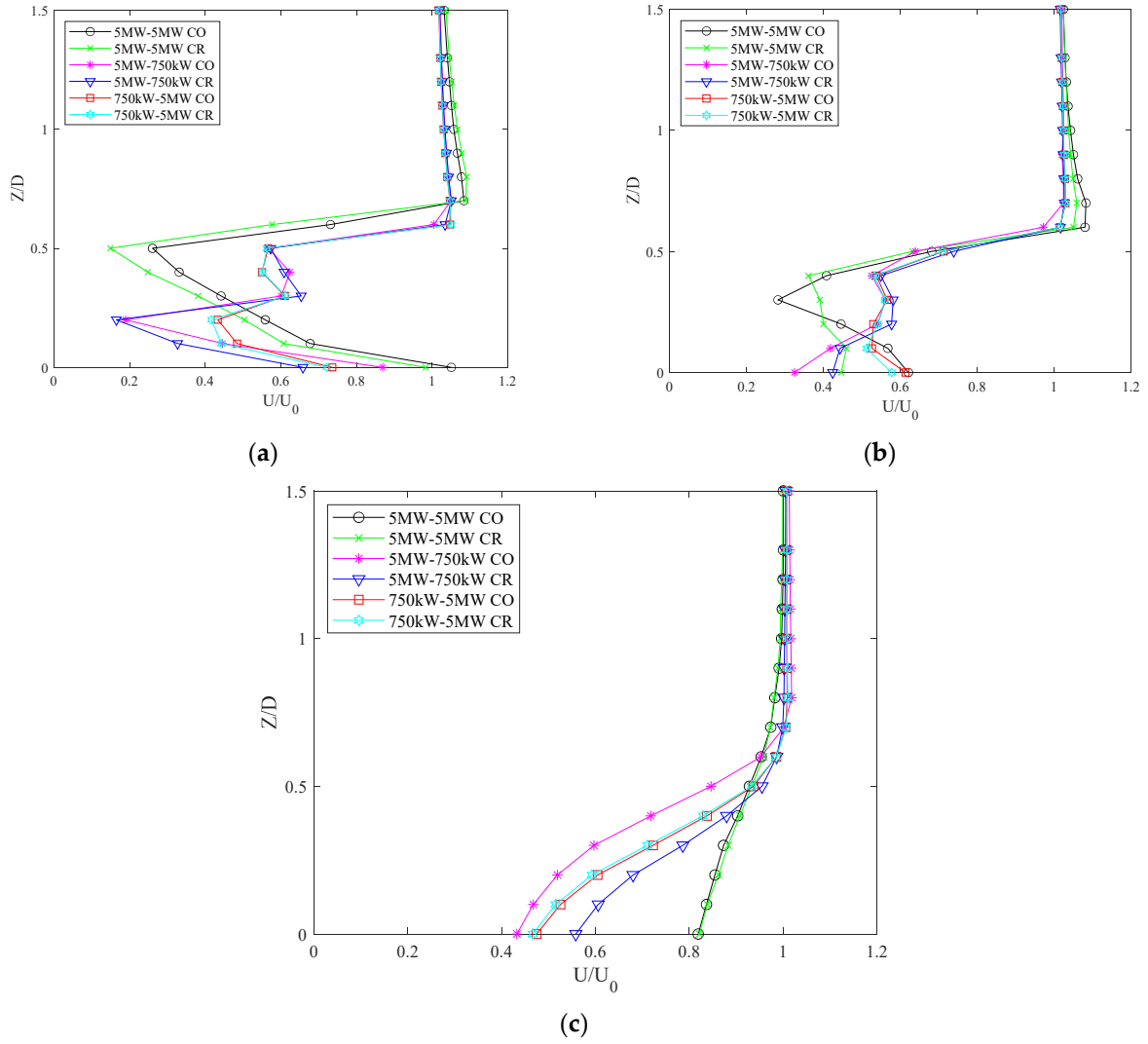

Figure 11. Vertical profiles of streamwise velocity at variant locations in wake flows (**a**) X/D = 1.0; (**b**) X/D = 2.0; (**c**) X/D = 3.0.

Compared with 5 MW-750 kW and 750 kW-5 MW DRWTs, the 5 MW-5 MW CO-DRWT and CR-DRWT gave a larger velocity deficit in wake flow. This is consistent with what has been mentioned in Section 3.1; the 5 MW-5 MW CO-DRWT and 5 MW-5 MW CR-DRWT had a higher normalized power coefficient. In DRWTs composed of 750 kW and 5 MW SRWTs, the downwind rotor of the DRWTs made use of the induced velocity in the upwind rotor wake in CR-DRWTs to produce about 10% more power output. Therefore, the velocity deficit in 5 MW-750 kW and 750 kW-5 MW CR-DRWTs was more significant than that in 5 MW-750 kW and 750 kW-5 MW CO-DRWTs.

A banded high-velocity region with a length of (1–2) D was found behind the tip of the DRWT blades. The high-velocity region in the wake was axisymmetric in steady inflow. It radiated outward in a circle, dissipated rapidly, and expanded within the range of the near wake. The high-velocity wake at the tip of the blade was caused by the wake vortex containing high turbulence.

The high-velocity regions in the wake caused by high turbulent kinetic energy at the blade tip of the 5 MW-5 MW CO-DRWT and 5 MW-5 MW CR-DRWT were stronger than those of 5 MW-750 kW and 750 kW-5 MW DRWTs. In addition, there was a faster velocity deficit recovery speed in 5 MW-5 MW DRWTs. In Figure 10c, 5 MW-5 MW CR-DRWT and 5 MW-5 MW CO-DRWT velocity profiles in the wake recover to 0.8 times the inflow wind speed. The 5 MW-5 MW DRWTs have a higher velocity deficit recovery speed. The length

required for the wake velocity recovery is shorter. The high kinetic energy in the wake at the blade tip replenished the energy in the velocity deficit region. The mixing of the trailing vortices at the tip of the DRWT blade produced a high kinetic energy region, especially in 5 MW-5 MW DRWTs. The recovery distance required for the velocity deficit of the DRWT was reduced.

4.3. Trailing Vortex Structure

In wind farms when the wind turbines work in a cluster, the wake recovery speed of the front rotors directly affects the power conversion of the rear rotors. Franz et al. [29] investigated the effect of the rotation direction of an SRWT on the rear SRWT when the rotors lined up in an array. The wake characteristics of the front wind turbine will affect the operation of the rear wind turbine. This section gives the results of the vortex of DRWTs and explains the progress of the tip and root vortex mixing and merging of DRWTs.

Figure 12 shows the tip and root vortices formed by the rotor rotations, as well as the shedding, mixing and dissipation processes. The tip and root vortices of DRWTs have the same helical structure as those of an SRWT. The vortices are mainly concentrated at the tip and root of the upwind and the downwind rotors, but the special feature of the DRWT vortices lies in the interaction of the upwind rotor and downwind rotor vortices.

The length of the vortices of the 5 MW-5 MW DRWTs was shorter than the DRWTs composed of 750 kW and 5 MW rotors. This is in line with the results observed in Figure 10a,b of the wake velocity distribution. In the wake velocity distribution of 5 MW-5 WM DRWTs, there were circular high-velocity regions radiating outward from the blade tip. This corresponds to the high-velocity flow generated by the vortices shown in Figure 13a,b. The velocity deficit's quick recovery benefited from the flow with high turbulent kinetic energy. Therefore, it can be concluded that the rapid recovery of the velocity deficit is caused by the mixing and merging of the two rotors' vortices.

Being different from 5 MW-5 WM DRWTs, the trailing vortices of 5 MW-750 kW and 750 kW-5 MW DRWTs were not at the same height. The different diameters of the upwind rotor and the downwind rotor kept from mixing the vortices generated at the blade tip. The trailing vortices of 5 MW-750 kW DRWTs dissipated faster in the form of mutual interference. It can be seen in Figure 10c that the trailing vortex of the upwind rotor of the 5 MW-750 kW CO-DRWT wraps the trailing vortex of the downwind rotor inside. The directions of rotation of the downwind rotor and upwind rotor are the same. Two trailing vortices rotate in the same direction, enhancing the rapid dissipation of the vortices after a short distance. It is difficult for vortices to maintain their original spiral structures. The vortices generated by the CR-DRWT also have the same evolution trend, but it is not as obvious as that generated by the CO-DRWT.

The vortices generated by the upwind rotor of 750 kW-5 MW DRWTs pass through the downwind rotor and are disturbed by the rotation of the downwind rotor. The vortices generated by the upwind rotor dissipate after passing through the downwind rotor. The turbulent flow caused by the trailing vortex of the upwind rotor reduces the wind energy capture efficiency of the downwind rotor. As a result, the downwind rotor has a significant decrease in power output. The downwind rotor power output is reduced to 90% of the power output of the 5 MW SRWT. In contrast, the upwind rotor of the 5 MW-750 kW DRWT still retains 95% of its power output relative to the 5 MW SRWT.

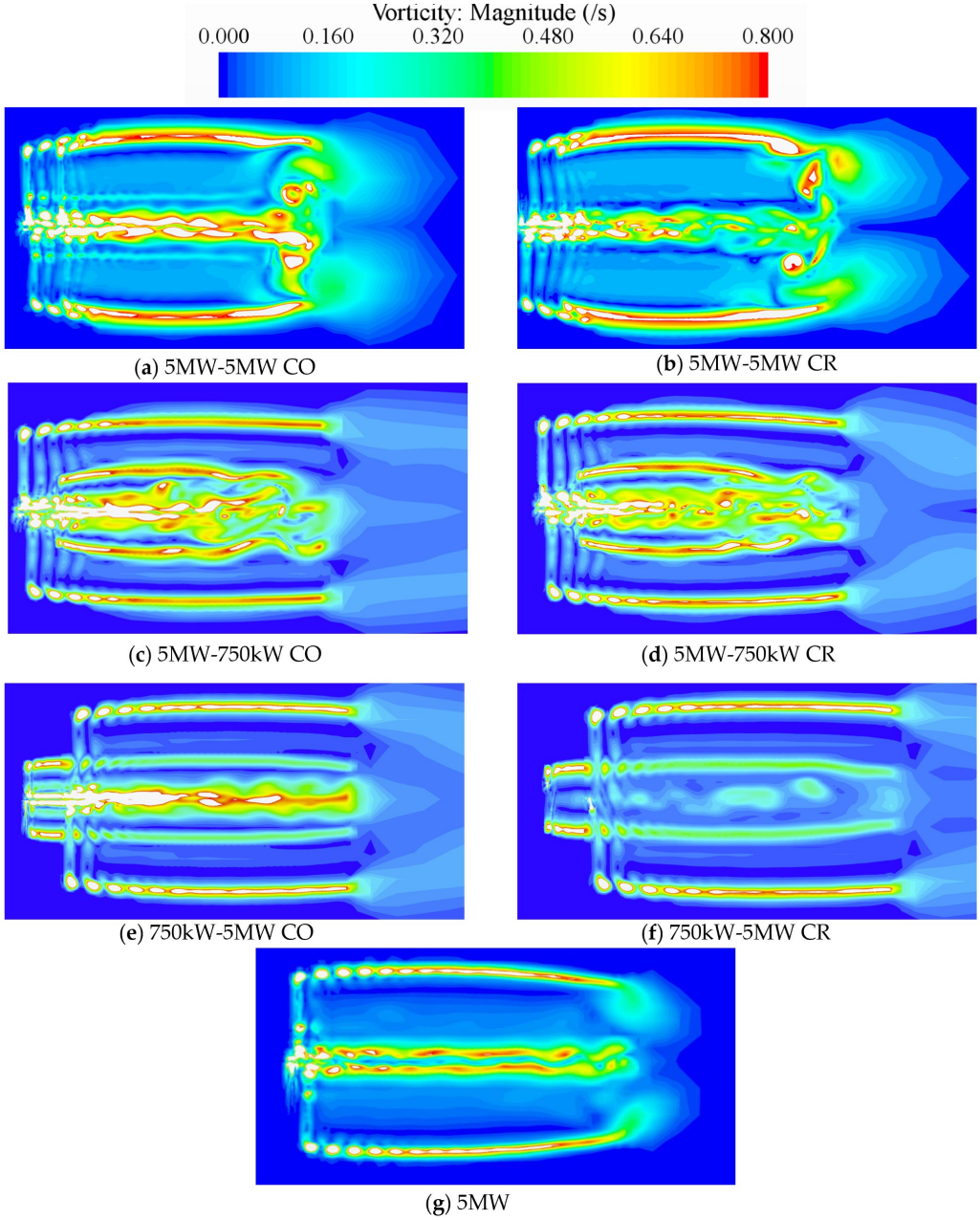

Figure 12. Instantaneous vorticity field in profile of DRWTs and 5 MW SRWT.

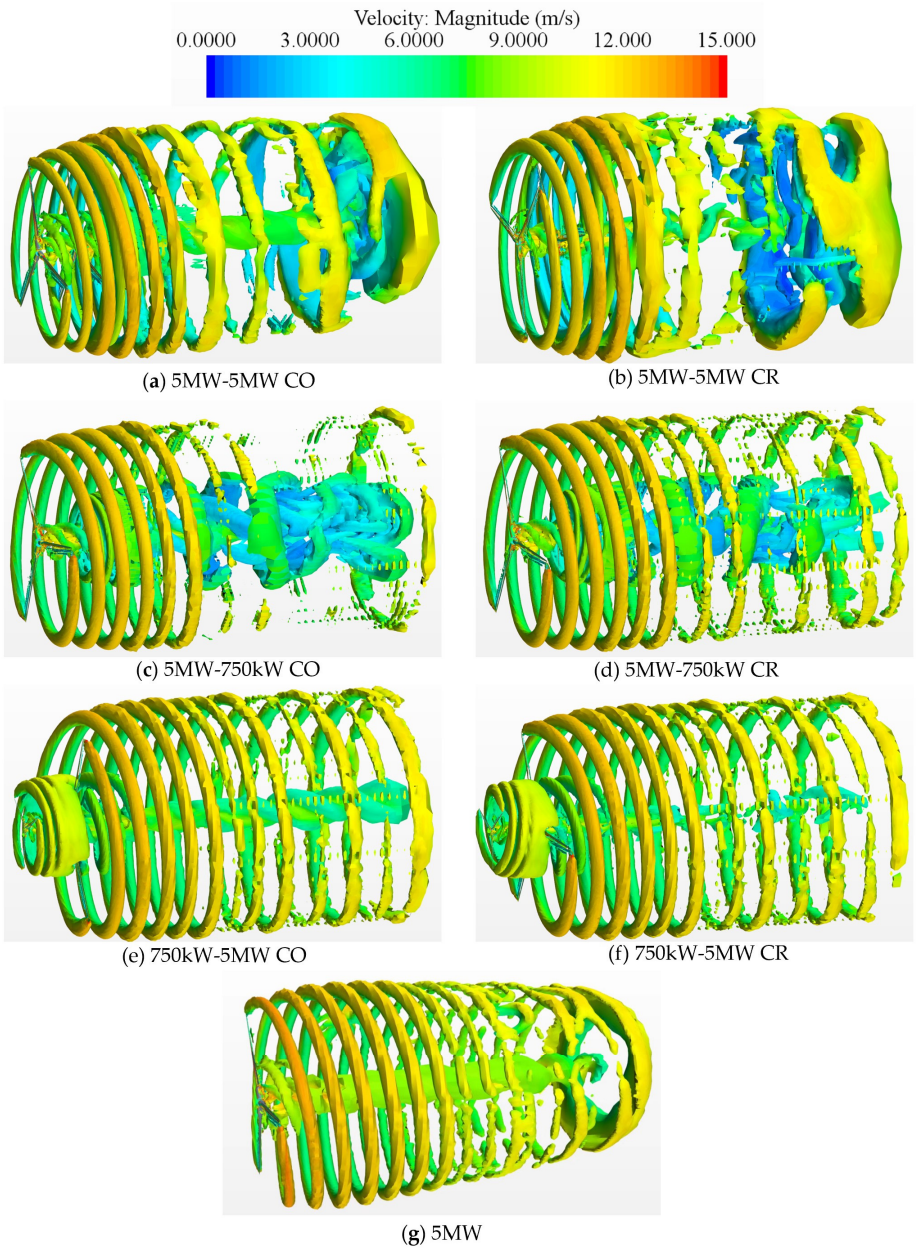

Figure 13. The trailing vortices of DRWTs and 5 MW SRWT.

5. Conclusions

In this study, dual-rotor wind turbines (DRWTs) were proposed by composing three different sizes (5 MW-5 MW, 5 MW-750 kW and 750 kW-5 MW) with both co-rotating and counter-rotating configurations based on the NREL Offshore Baseline-5 MW and NREL 750 kW wind turbines. Numerical simulations based on the computational fluid dynamics (CFD) method were carried out by setting the k-ω SST RANS turbulence model for the solution model. The inlet flow was set to a steady flow of 11.4 m/s and the rotating rates were set to the same rotating speed as of a single wind turbine. The power performance and aerodynamic characteristics of the DRWTs were calculated and compared. The flow phenomena in the wake of the DRWTs, including the velocity distribution and the trailing vortices, were also analyzed.

The power coefficients and thrust coefficients of 5 MW-5 MW, 5 MW-750 kW and 750 kW-5 MW CO-DRWTs and CR-DRWTs were normalized and investigated with reference to the power coefficient of the 5 MW SRWT. In addition, the individual power coefficient variations of the upwind and downwind rotors of the 5 MW-5M, 5 MW-750 kW

and 750 kW-5 MW CO-DRWTs and CR-DRWTs with the corresponding single rotor power were given. The power solidity ratio was used to evaluate the power efficiency of 5 MW-5 MW, 5 MW-750 kW and 750 kW-5 MW CO-DRWTs and CR-DRWTs. Meanwhile, the wake velocity plane distributions and wake vortex structures were also given for 5 MW-5 MW, 5 MW-750 kW and 750 kW-5 MW CO-DRWTs and CR-DRWTs. The velocity and vortex results were used to compare the wake characteristics and the evolution of the non-constant tip and root vortices for different DRWTs. The correlation between the velocity deficit and power coefficient of the DRWT was explained, along with the causal relationship between the faster wake velocity deficit recovery rate and wake vortex evolution of the CR-DRWT.

The DRWTs have improved power coefficients compared with the SRWTs. The power coefficient of the 5 MW-5 MW CO-DRWT is 1.22 times higher than that of the 5 MW SRWT. Comparing the DRWTs' upwind rotors and downwind rotors with the SRWTs', the individual-rotor power has a small decline due to the velocity deficit caused by the rotation and the negative impact of the two rotors' rotation. In addition, the results of the power density ratio show that the 5 MW-750 kW CR-DRWT is a more reasonable configuration because using the 5 MW rotor as the upwind rotor can avoid the negative influence of the trailing vortices of the upwind rotor on the downwind rotor. It is also worth mentioning that the added rotor and increase in aerodynamic load can cause additional costs for the supporting structure. The economic evaluation can be further studied by comparing the cost increase of structures with the increased power from DRWTs deployed in a wind farm.

In the wake flow of the DRWT, it is found that the 5 MW-5 MW DRWT has a faster velocity deficit recovery speed, which is related to vortices mixing with each other at the tip of the blades. The velocity of the 5 MW-5 MW DRWTs in the wake can recover to 0.8 U0 in a 3 D distance. The results of the vortices show that the upwind rotor and downwind rotor blade tip vortex systems interfere with each other. The energy generated from the merging and mixing of the vortices compensates for the rotor wake velocity deficit. Avoiding the trailing vortex of the upwind rotor from directly acting on the downwind rotor can effectively prevent the decline of the power coefficient of the downwind rotor.

Author Contributions: Conceptualization, K.W., T.L. and M.C.O.; methodology, K.W., T.L., Y.W. and M.C.O.; software, K.W.; validation, K.W., T.L., Y.W. and M.C.O.; formal analysis, K.W., T.L., Y.W., M.C.O. and T.W.; writing—original draft preparation, K.W., T.L. and Y.W.; writing—review and editing, K.W., T.L., Y.W., M.C.O. and T.W.; project administration, K.W.; funding acquisition, K.W. All authors have read and agreed to the published version of the manuscript.

Funding: This research was funded by the National Natural Science Foundation of China, grant number 52171289; Key Area R&D Program of Guangdong Province, China, grant number 2021B0101200002; Natural Science Foundation of Guangdong Province, China, grant number 2021A1515011771.

Institutional Review Board Statement: Not applicable.

Informed Consent Statement: Not applicable.

Data Availability Statement: Not applicable.

Conflicts of Interest: The authors declare no conflict of interest.

References

1. Abdelilah, Y.; Bahar, H.; Criswell, T.; Bojek, P.; Briens, F.; Feuvre, P.L. *Renewables 2020 Analysis and Forecast to 2025*; IEA: Paris, France, 2020.
2. Prakash, G.; Anuta, H. *Future of Wind: Deployment, Investment, Technology, Grid Integration and Socio-Economic Aspects*; International Renewbale Energy Agency: Abu Dhabi, United Arab Emirates, 2019.
3. Breton, S.-P.; Moe, G. Status, plans and technologies for offshore wind turbines in Europe and North America. *Renew. Energy* **2009**, *34*, 646–654. [CrossRef]
4. Lee, J.; Zhao, F. *Global Offshore WindReport 2021*; Global Wind Energy Council: Brussels, Belgium, 2020.
5. Fang, Y.; Duan, L.; Han, Z.; Zhao, Y.; Yang, H. Numerical analysis of aerodynamic performance of a floating offshore wind turbine under pitch motion. *Energy* **2020**, *192*, 116621. [CrossRef]
6. Wang, K.; Moan, T.; Hansen, M.O.L. A Method for Modeling of Floating Vertical Axis Wind Turbine. In Proceedings of the 32nd International Conference on Ocean, Offshore and Arctic Engineering, Nantes, France, 9–14 June 2013; Volume 8.

7. Borg, M.; Wang, K.; Collu, M.; Moan, T. A Comparison of Two Coupled Model of Dynamics for Offshore Floating Vertical Axis Wind Turbines (VAWT). In Proceedings of the 33rd International Conference on Ocean, Offshore and Arctic Engineering, San Francisco, CA, USA, 8–13 June 2014; Volume 9A.
8. Manwell, J.F.; McCowan, J.G.; Rogers, A.L. Wind Energy Explained: Theory, design and application. *Wind. Eng.* **2009**, *30*, 169–170.
9. Tony, B.; Nick, J.; David, S.; Ervin, B. *Wind Energy Handbook*; John Wiley & Sons, Ltd.: Hoboken, NJ, USA, 2011.
10. Newman, B.G. Actuator-disc theory for vertical-axis wind turbines. *J. Wind. Eng. Ind. Aerodyn.* **1983**, *15*, 347–355. [CrossRef]
11. Ozbay, A.; Tian, W.; Hu, H. An Experimental Investigation on the Aeromechanics and Near Wake Characteristics of Dual-Rotor Wind Turbines (DRWTs). In Proceedings of the 32nd ASME Wind Energy Symposium, National Harbor, MD, USA, 13–17 January 2014.
12. Wang, Z.; Ozbay, A.; Tian, W.; Hu, H. An experimental study on the aerodynamic performances and wake characteristics of an innovative dual-rotor wind turbine. *Energy* **2018**, *147*, 94–109. [CrossRef]
13. Rosenberg, A.; Selvaraj, S.; Sharma, A. A Novel Dual-Rotor Turbine for Increased Wind Energy Capture. In Proceedings of the Science of Making Torque from Wind 2014 (TORQUE 2014), Copenhagen, Denmark, 18–20 June 2014; p. 012078.
14. Lee, S.; Kim, H.; Lee, S. Analysis of aerodynamic characteristics on a counter-rotating wind turbine. *Curr. Appl. Phys.* **2010**, *10*, S339–S342. [CrossRef]
15. Cho, W.; Lee, K.; Choy, I.; Back, J. Development and experimental verification of counter-rotating dual rotor/dual generator wind turbine: Generating, yawing and furling. *Renew. Energy* **2017**, *114*, 644–654. [CrossRef]
16. Farahani, E.M.; Hosseinzadeh, N.; Ektesabi, M. Comparison of fault-ride-through capability of dual and single-rotor wind turbines. *Renew. Energy* **2012**, *48*, 473–481. [CrossRef]
17. Vasel-Be-Hagh, A.; Archer, C.L. Wind farms with counter-rotating wind turbines. *Sustain. Energy Technol. Assess.* **2017**, *24*, 19–30. [CrossRef]
18. Mitulet, L.-A.; Oprina, G.; Chihaia, R.-A.; Nicolaie, S.; Nedelcu, A.; Popescu, M. Wind Tunnel Testing for a New Experimental Model of Counter-rotating Wind Turbine. *Procedia Eng.* **2015**, *100*, 1141–1149. [CrossRef]
19. Abohamzeh, E.; Jamil, M.; Benim, A.C. Prediction of aeroacoustic performance of counter-rotating wind turbine by changing the rotational speed of front rotor. *SN Appl. Sci.* **2020**, *2*, 86. [CrossRef]
20. Wang, L.; Quant, R.; Kolios, A. Fluid structure interaction modelling of horizontal-axis wind turbine blades based on CFD and FEA. *J. Wind. Eng. Ind. Aerodyn.* **2016**, *158*, 11–25. [CrossRef]
21. Lefebvre, S.; Collu, M. Preliminary design of a floating support structure for a 5MW offshore wind turbine. *Ocean. Eng.* **2012**, *40*, 15–26. [CrossRef]
22. Sang, S.; Wen, H.; Cao, A.X.; Du, X.R.; Zhu, X.; Shi, Q.; Qiu, C.H. Dynamic modification method for BEM of wind turbine considering the joint action of installation angle and structural pendulum motion. *Ocean. Eng.* **2020**, *215*, 107528. [CrossRef]
23. Onel, H.C.; Tuncer, I.H. Investigation of wind turbine wakes and wake recovery in a tandem configuration using actuator line model with LES. *Comput. Fluids* **2021**, *220*, 104872. [CrossRef]
24. Celik, Y.; Ma, L.; Ingham, D.; Pourkashanian, M. Aerodynamic investigation of the start-up process of H-type vertical axis wind turbines using CFD. *J. Wind. Eng. Ind. Aerodyn.* **2020**, *204*, 104252. [CrossRef]
25. Rocha, P.A.C.; Rocha, H.H.B.; Carneiro, F.O.M.; da Silva, M.E.V.; de Andrade, C.F. A case study on the calibration of the k–ω SST (shear stress transport) turbulence model for small scale wind turbines designed with cambered and symmetrical airfoils. *Energy* **2016**, *97*, 144–150. [CrossRef]
26. Rocha, P.A.C.; Rocha, H.H.B.; Carneiro, F.O.M.; Vieira da Silva, M.E.; Bueno, A.V. k–ω SST (shear stress transport) turbulence model calibration: A case study on a small scale horizontal axis wind turbine. *Energy* **2014**, *65*, 412–418. [CrossRef]
27. Rahimian, M.; Walker, J.; Penesis, I. Numerical assessment of a horizontal axis marine current turbine performance. *Int. J. Mar. Energy* **2017**, *20*, 151–164. [CrossRef]
28. CD-adapco. *STAR-CCM+ 11.0 User Guide*; Siemens, Inc.: Berlin, Germany, 2016.
29. Chorin, A.J. Numerical solution of the Navier-Stokes equations. *Math. Comput.* **1968**, *22*, 745–762. [CrossRef]
30. Lee, S.; Son, E.; Lee, S. Velocity interference in the rear rotor of a counter-rotating wind turbine. *Renew. Energy* **2013**, *54*, 235–240. [CrossRef]